PERFORMANCE OF ACOUSTIC METAMATERIAL BASED ON A DOUBLE LAYER MICROPERFORATED PANEL

Linconl C. B. Farias[1], Gildean do N. Almeida[1], Erasmo F. Vergara[1], Leandro R. Barbosa[1], Robson Z. Mikulski[1]

[1]*Laboratory of Vibrations and Acoustics, Mechanical Engineering Department, Federal University of Santa Catarina*
R. Eng. Agronômica Andrei C. Ferreira, s/n-Trindade, 88040 - 900, Florianópolis-SC, Brazil
linconlcesar@hotmail.com, gildean_fsa@hotmail.com, e.f.vergara@ufsc.br

Abstract. In recent years, the development of models of acoustic metamaterials has received considerable prominence due to the several unique properties found in this absorbers. AMM based on a microperforated panel of type with internal air cavities have been promising and depending on the application provide satisfactory results at low frequencies. This work investigates the performance of a honeycomb type acoustic metamaterial (AMM) modeled as double-layered microperforated panels. The effective sound absorption in the frequency range between 100 and 500 Hz is verified analytical, numerical and experimentally. The analytical results are corroborated numerically using a 3D finite element (FEM) method. A sound absorber sample was manufactured using 3D printing technology and evaluated in an impedance tube considering the normal incidence of waves. Sound absorption of 94% at 182 Hz with a bandwidth of 52 Hz was obtained and good agreement with the analytical model was reached. In addition, it is verified that this result is due to the high dissipation of sound energy in the perforation region of the first panel. Therefore, this sound absorber shows excellent performance to control the low frequencies.

Keywords: Sound absorption, Acoustic metamaterial, Low-frequency, Double-layered.

1 Introduction

In recent years, the development of acoustic metamaterials (AMM) models has received considerable attention due to the exceptional characteristics and properties found in these absorbers [1]. In the 1970s, studies capable of describing the behavior of perforated panels were already highlighted [2], since designing absorbers with specific characteristics as alternatives to traditional porous materials was necessary. Absorber structures composed of double perforated panels were also proposed for applications where sound absorption was not limited to certain frequency ranges only. In addition, absorbers with micro-perforated panel coupled to air cavities gained visibility due to their performance at low frequencies [3, 4], which made them useful in several applications.

On the other hand, AMMs, through their characteristics and properties derived from their geometric arrangement, have provided a way for an efficient control of the sound energy related to low frequencies[5]. In this sense, acoustic metamaterials based on microperforated panels with different types of perforations have been frequently proposed [6, 7]. Almeida *et al.* [5] proposed an absorber based on the concept of symmetrical rolled spaces coupled to a panel with a micro-slit of variable thickness and achieved excellent low-frequency sound absorption with extended bandwidth. The effect of different geometries in the perforation of a panel on the sound absorption behavior of an acoustic metamaterial were discussed and presented by Almeida *et al.* [6].

In this work, analytical, numerical and experimental studies of the sound absorption behavior of a honeycomb-type AMM based on double-layer micro-perforated panels in the frequency range between 100 and 500 Hz is reported. It is analytically and numerically demonstrated that the influence of the first perforated panel on the absorber behavior is prominent. An absorber sample is fabricated using 3D printing technology and experimentally analyzed in an impedance tube apparatus. The results obtained in the experiment are in good agreement with the theoretical model and demonstrate that the absorber design has applications in dfferent applications of acoustics.

2 Structure of the absorber

The structure of a unit cell composed of a double microperforated panel and its respective geometric parameters is illustrated in Fig. 1 . We can see that the unit cell has width $X1$, depth $X2$ and height $X3$. The perforation of panels 1 and 2 have diameter $d1$ and $d2$, respectively, and thickness $t1$ and $t2$. Air cavities 1 and 2 have depth H and $b2$, respectively. The height and width of pocket 1 is $b1$ and pocket 2 are $b1$ and H, respectively. Interior walls are $tw/2$ thick. Finally, T is the hard back panel that prevents sound leakage.

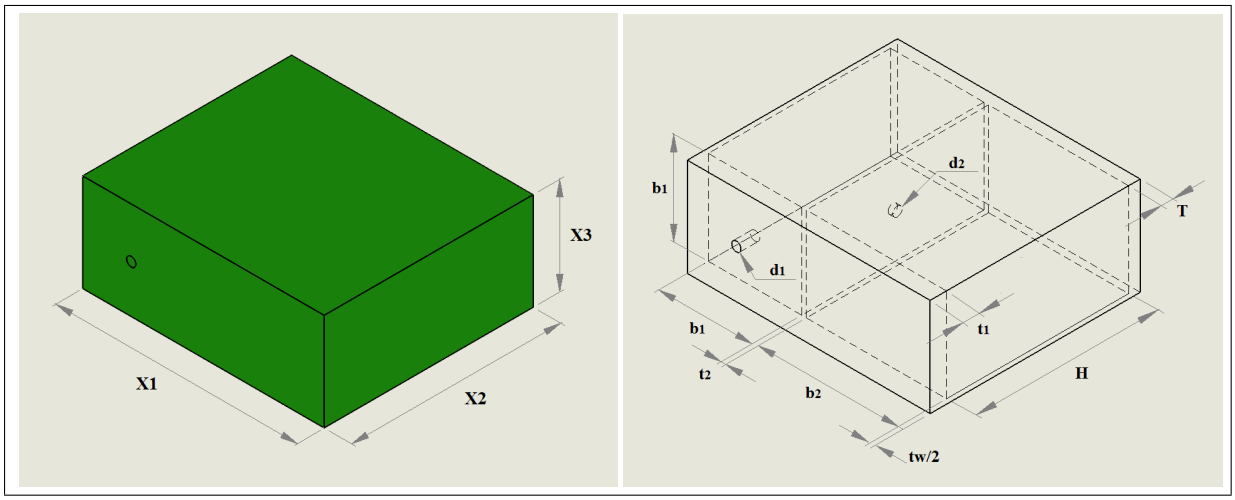

Figure 1. The sketch the structure of the acoustic metamaterial AMM

2.1 Theoretical method

In general, the sound absorption coefficient of an AMM when the absorber is supported by a rigid wall can be obtained with [8],

$$\alpha = 1 - \left| \frac{Z_s - Z_0}{Z_s + Z_0} \right|^2 . \tag{1}$$

Where $Z_0 = \rho_0 c_0$ is the impedance of the air, with $c_0 = 343$ [m/s^2] and $\rho_0 = 1.21$ [kg/m^3] represent the velocity and density of air, respectively. $Z_s = \delta_s(Z_{Pn} + \delta_n Z_{Cn})$ is the total impedance of the system, with $\delta_s = (b_1 + b_2 + t_w + t_2) / (b_1 + t_w)$ and $\delta_n = b_1^2 / (b_1 D_1)$ representing the area and surface modifying factors, respectively. Z_{Pn} is the approximate impedance of the n-th panel, which is given by [8, 9],

$$Z_{P_n} = \frac{32\eta t_n}{P_n d_n^2} \left[\left(1 + \frac{y_n^2}{32} \right)^{0.5} + \frac{\sqrt{2} y_n^2 d_n}{32 t_n} \right] + \frac{j\rho_0 \omega t_n}{P_n} \left[1 + \left(9 + \frac{y_n^2}{2} \right)^{-0.5} + \frac{0.85 d_n}{t_n} \right], \tag{2}$$

where $\eta = 1.814 \times 10^{-5}$ [Pa·s] is the viscosity of air and $y_n = d_n \sqrt{(\rho_0 \omega / 4\eta)}$ is the ratio of the perforation diameter [2, 9]. P_n is the porosity of the panel, which when $n = 1$ can be obtained by $P_1 = \pi (d_1/2)^2 / (b_1 + t_w)^2$, when n is greater than 1, $P_n = \pi (d_1/2)^2 / (b_1)^2$. The impedance of the air cavity Z_{C_n} is given by,

$$Z_{Cn} = Z_0 \frac{(Z_{n+1}) \cos(kD_n) + j Z_0 \sin(kD_n)}{Z_0 \cos(kD_n) + j (Z_{n+1}) \sin(kD_n)}, \tag{3}$$

which becomes $Z_{Cn} = -jZ_0 \cot(kD_n)$ when $n = 2$ and $k = \omega/c_0$ represents the number of waves. According to Fig. 1 the two cavities have thickness $D_1 = H$ and $D_2 = b_2$, respectively. Note that the area modification factor for the first layer, or $n = 1$, is equal to $\delta_1 = (t_w + b_1)^2 / b_1^2$ and for $n > 1$ is obtained by δ_n.

2.2 Numerical analysis by FEM

A numerical analysis using the finite element method (FEM) was performed in COMSOL Multiphysics software to corroborate the behavior of the AMM. In this sense, a virtual impedance tube experiment was carried out in the frequency domain and the multiphysics interaction between the Acoustic and Thermoacoustics modules was adopted. All system walls are considered rigid, a 1 Pa sound pressure source was introduced at one end of the tube with the AMM sample located at the opposite end. In the numerical model, we use the normative model ISO 10534-2:1998 [10] as a reference, that is, the pressure (P_i) and particle velocity (v_i) responses were obtained and recorded at two different points, then we determine the acoustic impedance ($Z_i = Pi/v_i$) and calculate the sound absorption coefficient in the numerical model $\alpha_i = 1 - |Z_i - Z_0/(Z_i + Z_0)|^2$. The governing equations in the process include the linearized Navier-Stokes equation, the energy and continuity equations, and the equation of state for an ideal gas [11],

$$\rho_0 \frac{\partial \mathbf{v}}{\partial t} = -\nabla P + \left(\frac{4}{3}\eta + \mu_B\right)\nabla(\nabla \cdot \mathbf{v}) - \eta \nabla \times (\nabla \times \mathbf{v}),$$

$$\rho_0 C_p \frac{\partial T}{\partial t} = \frac{\partial P}{\partial t} + \kappa \nabla(\nabla T),$$

$$\frac{\partial \rho}{\partial t} = -\rho_0 \nabla \cdot \mathbf{v},$$

$$P = \rho R_0 T, \tag{4}$$

where $\mathbf{v}$, ρ, P, T, μ_B, κ, C_p and R_0 represent, respectively, the velocity vector, air density, pressure, temperature, bulk viscosity [1.21×10^{-5} Pa·s], thermal conductivity, heat capacity at constant pressure [1007 Jkg^{-1}K^{-1}] and gas constant [8.32 Jmol^{-1}K^{-1}].

3 Results and discussions

3.1 Analytical and numerical results

The absorber behavior was analyzed with the implementation of the sound absorption coefficient for two different models, the geometric parameters used in the analysis are listed in Table 1 . The Fig. 2 shows the theoretical behavior of different models of the absorber. Sound absorption peaks are located with their respective amplitudes at 331 Hz (0.999) and 264 Hz (0.990) for model 1 and 2, respectively. Although the models have different geometric parameters that make them operate at different frequencies, the bandwidth at 50 % of the maximum absorption remains almost constant, that is, 72 Hz and 73 Hz for models 1 and 2 , respectively. Also, the ratio between bandwidth and frequency is 21.75 % and 27.65 %, correspondingly. The comparison of the sound absorption coefficient determined from analytical and numerical methods are shown in Fig. 2 and good agreement between methods is verified in both models of the absorber, which confirms the validity of the both methods.

Table 1. Parameters (in mm) used in the analysis.

Parameters	d_1	d_2	t_1	t_2	D_1	D_2	b_1	tw
Model 1	1.6	1.6	2.0	2.0	20.0	20.0	15.0	0.5
Model 2	1.5	2.0	2.0	1.0	33.0	20.0	15.0	0.5

The excellent behavior of the absorber can be better understood from the strong coupling of the total impedance of the system with that of the air impedance. For this class of absorber, strong coupling occurs when the real part

of the total system impedance normalized by the air impedance tends to the unit value and its imaginary part to zero.The bottom of Fig. 3 represents the behavior of the parts of the AMM total impedance for both models. Note that at the operating frequencies of models 1 and 2 the imaginary parts are zero. Meanwhile the real parts are 1.06 and 0.865 respectively. Furthermore, note that maximum sound absorption is mainly achieved in model 1, whose real part is almost unity, which demonstrates a strong coupling of the model total impedance with the air impedance.

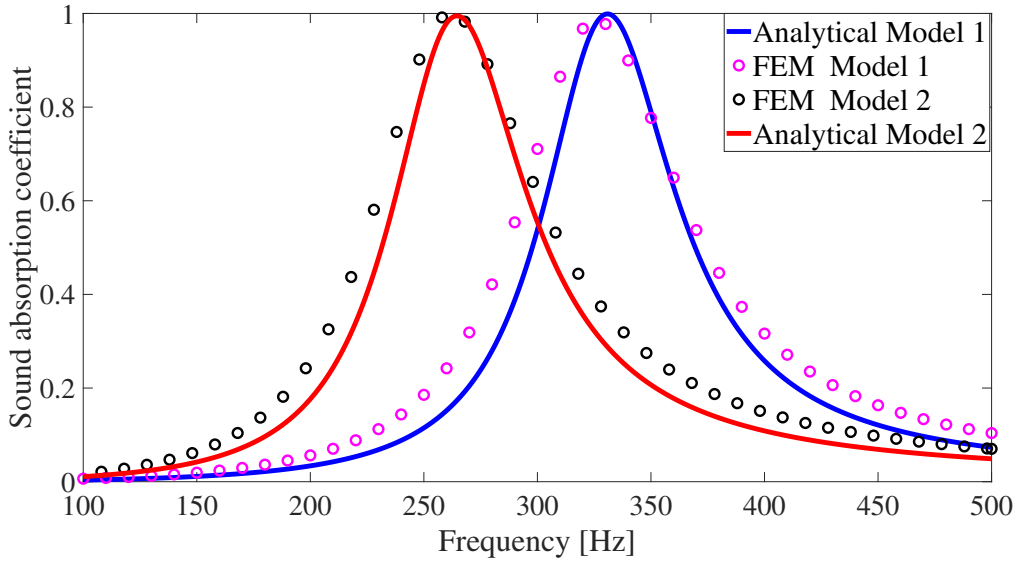

Figure 2. Analytical and numerical behavior of sound absorption coefficient for distincts models

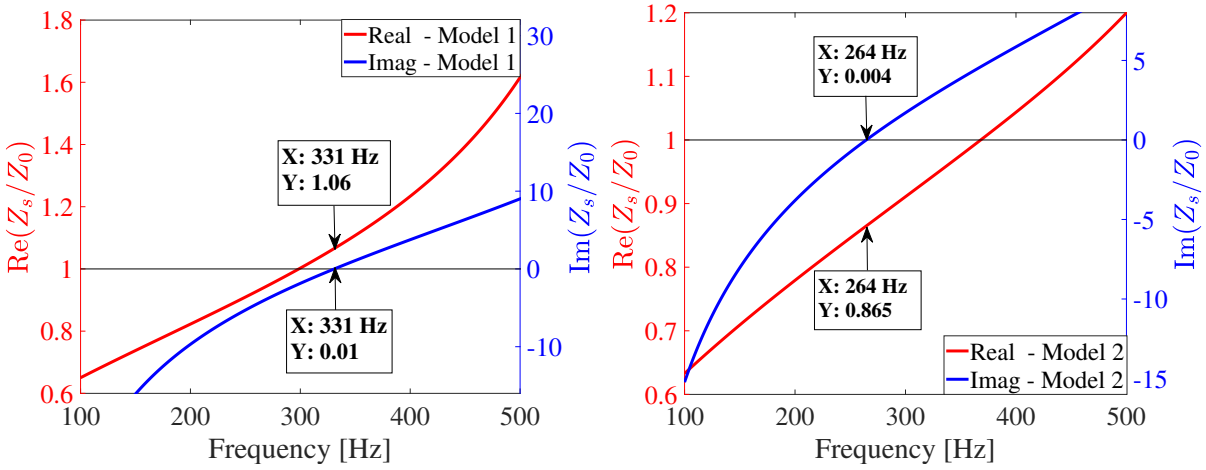

Figure 3. Normalized total impedance behavior of the models

3.2 Experimental validation

The numerical and experimental validation of the performance of the sound absorption coefficient of an AMM sample was carried out. In the experimental test the standard two-microphone method was used considering an impedance tube with a cylindrical diameter of 107 mm [10]. In the construction of the absorber sample, the 3D printing technology with the material extrusion technique (FDM-fused deposition material) was used. The material

used in the manufacture of the sample was ABS (Acrylonitrile Butadiene Styrene). A schematic and fabricated sample are illustrated in Fig. 4. The geometric parameters used in manufacturing are listed in Table 2 .

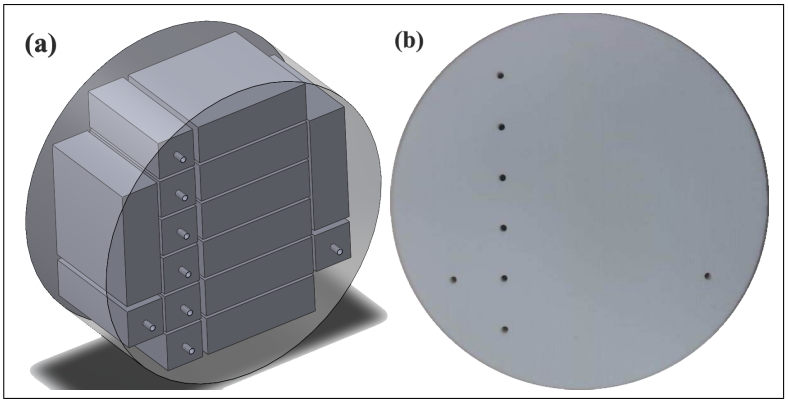

Figure 4. (a): Design of the structure consisting of 8 unit cells, (b): Structure built with 3D technology for experiment

Table 2. Parameters (in mm) used in manufacture of the sample and analysis.

Parameters	d_1	d_2	t_1	t_2	D_1	D_2	b_1	tw
Value	2.0	2.0	4.0	2.5	38.5	41.0	13.0	1.0

The Fig. 5 represents the theoretical, numerical and experimental behavior of the sample and a good agreement between the methods is evidenced. The sound absorption peaks and their respective amplitude are located at 188 Hz (0.998), 183 (0.993) Hz and 182 Hz (0.940), respectively. The bandwidth at 50% of the absorption maximum is 44 Hz, 47 Hz and 52 Hz for the theoretical, numerical and experimental models, respectively. The ratio between the bandwidth and the maximum absorption peak are 23.4%, 25.7% and 28.6%, correspondingly. Note that there is a small discrepancy in frequency and amplitude in the experimental method compared to numerical and theoretical methods, this difference is due to uncertainties arising from the sample manufacturing process [5, 6, 12]. Thus, based on the experimental bandwidth value and the operation frequency, it can be stated that the acoustic metamaterial acts as a deep-subwavelength absorber [13], since its total thickness is much smaller than the operation frequency wavelength, i.e., $\lambda/44$.

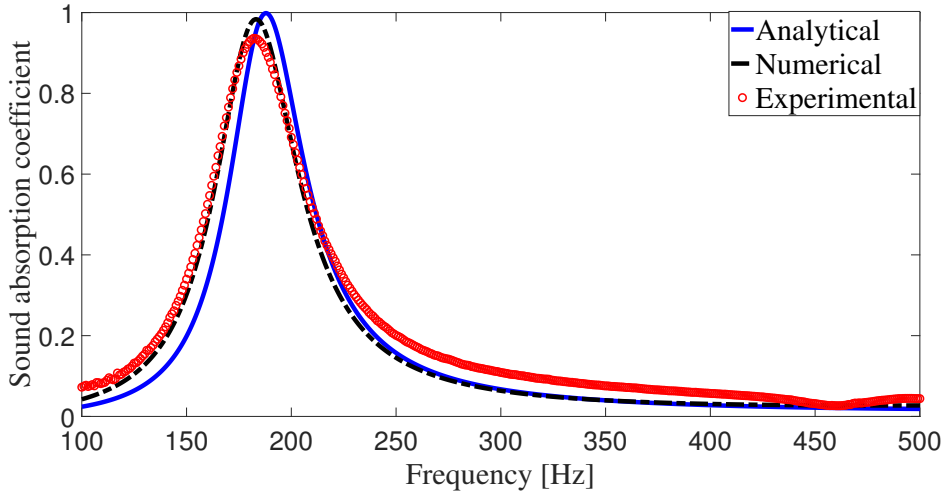

Figure 5. Theoretical, numerical and experimental behavior of the sound absorption coefficient

To understand the underlying mechanism of sound absorption of the AMM sample we also explore the possible paths of sound energy dissipation, i.e., thermal and viscous dissipation. In addition we mapped the acoustic pressure field at the operating frequency of a single cell only of the sample of the absorber since they are all the same. Figure 6 (c) illustrates the pressure field in the absorber, in which we can observe that the sound pressure is maximum at the end of the second cavity, intermediate in cavity 1 and minimum at the entrance of the panel, that is, in the microperforation. Thermal and viscous energy dissipation are illustrated in Fig. 6 (a) and (b), respectively. Viscous dissipation predominates over thermal effects, the first dissipation occurs in the region of the perforations of both panels, while the second in cavity 1 and mainly in the perforation of the second panel and cavity 2. In fact, the strong viscous dissipation is due to the air movement located in the edges and internally in the perforations be distorted due to the intense compression of the air in this region.

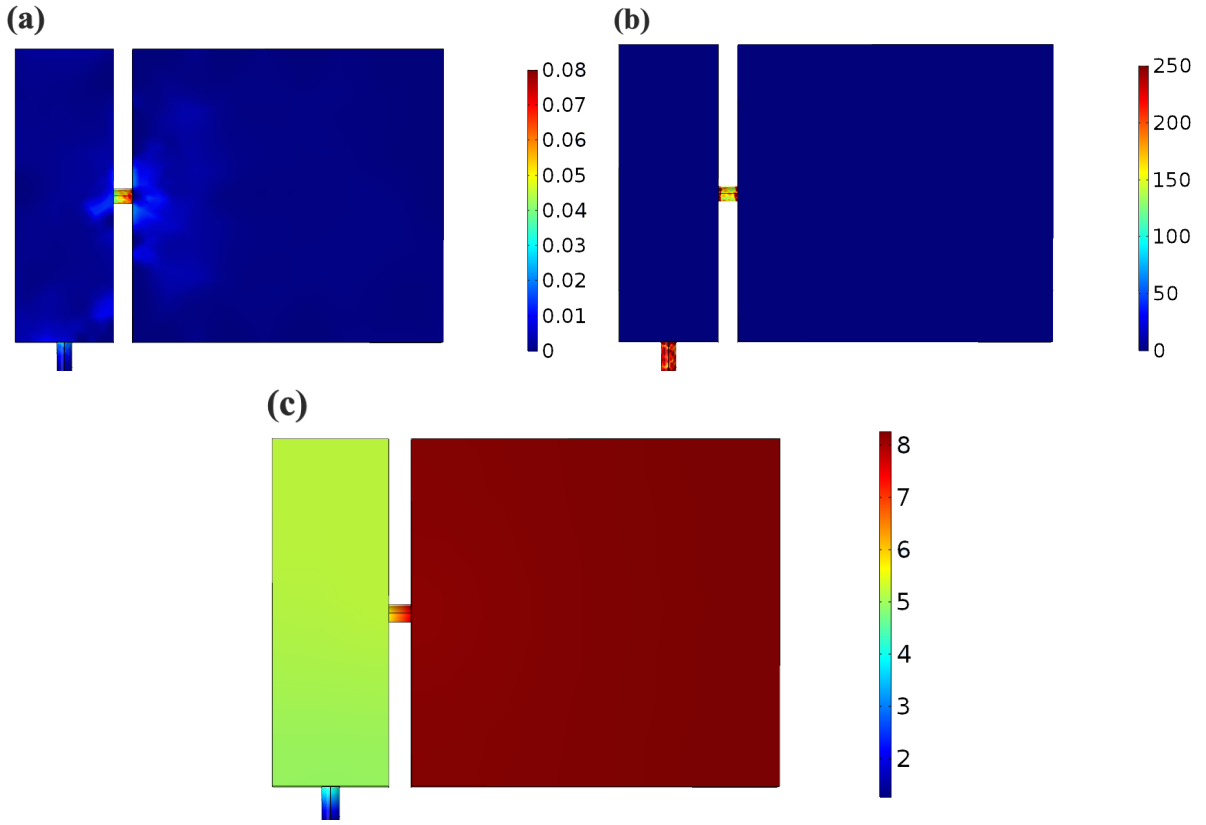

Figure 6. 2D contour of the energy dissipation and pressure field at the operating frequency 183 Hz. (a): Thermal dissipation energy [W/m^3], (b) Viscous dissipation energy [W/m^3], (c) Sound pressure field [Pa]

4 Conclusions

The behavior of an acoustic metamaterial composed of a double microperforated panel coupled to air cavities was presented and proved to be versatile for the control of low frequency sound absorption (100-500 Hz). Analytical and numerical models showed good agreement with the experimental verification of a sample manufactured using 3D printing technology. It was demonstrated that the effective sound absorption obtained at frequencies below $\leq$ 200 Hz is primarily due to the high dissipation of viscous sound energy in the region of the perforations of the panels. This performance makes the acoustic metamaterial an absorber with sub-wavelength scale, since its total depth ($t1 + D1$) is of the order of $\lambda/44$.

Acknowledgements. This work was carried out with the support of the Coordination for the Improvement of Higher Education Personnel (CAPES) of Brazil.

Authorship statement. The authors hereby confirm that they are the sole liable persons responsible for the au-

thorship of this work, and that all material that has been herein included as part of the present paper is either the property (and authorship) of the authors, or has the permission of the owners to be included here.

References

[1] K. Matlack, S. Krödel, A. Bauhofer, and C. Daraio. *Advanced Structured Composites as Novel Phononic Crystals and Acoustic Metamaterials*, pp. 155–162, 2016.
[2] D. Maa. Theory and design of microperforated panel sound-absorbing constructions, 1975.
[3] M. Dah-You. Design of microperforated panel constructions [j]. *Acta Acustica*, vol. 3, 1988.
[4] K. Sakagami, T. Nakamori, M. Morimoto, and M. Yairi. Double-leaf microperforated panel space absorbers: A revised theory and detailed analysis. *Applied Acoustics*, vol. 70, n. 5, pp. 703–709, 2009.
[5] G. Almeida, E. F. Vergara, L. R. Barbosa, and R. Brum. Low-frequency sound absorption of a metamaterial with symmetrical-coiled-up spaces. *Applied Acoustics*, vol. 172, pp. 107593, 2020.
[6] G. d. N. Almeida, E. F. Vergara, L. R. Barbosa, A. Lenzi, and R. S. Birch. A low-frequency sound absorber based on micro-slit and coiled cavity. *Journal of the Brazilian Society of Mechanical Sciences and Engineering*, vol. 43, n. 3, pp. 1–9, 2021.
[7] Y. Wang, H. Zhao, H. Yang, J. Zhong, D. Zhao, Z. Lu, and J. Wen. A tunable sound-absorbing metamaterial based on coiled-up space. *Journal of Applied Physics*, vol. 123, n. 18, pp. 185109, 2018a.
[8] Y. Tang, F. Xin, L. Huang, and T. Lu. Deep subwavelength acoustic metamaterial for low-frequency sound absorption. *EPL (Europhysics Letters)*, vol. 118, n. 4, pp. 44002, 2017.
[9] D.-Y. Maa. Potential of microperforated panel absorber. *the Journal of the Acoustical Society of America*, vol. 104, n. 5, pp. 2861–2866, 1998.
[10] ISO 10534-2:1998(E). Determination of sound absorption coefficient and impedance in impedance tubes – Part 2: Transfer-function method. Standard, International Organization for Standardization, 1998.
[11] W. BELTMAN. Viscothermal wave propagation including acousto-elastic interaction, part i: Theory. *Journal of Sound and Vibration*, vol. 227, n. 3, pp. 555–586, 1999.
[12] Y. Wang, H. Zhao, H. Yang, J. Zhong, D. Zhao, Z. Lu, and J. Wen. A tunable sound-absorbing metamaterial based on coiled-up space. *Journal of Applied Physics*, vol. 123, pp. 185109, 2018b.
[13] do G. N. Almeida, E. F. Vergara, L. R. Barbosa, A. Lenzi, and R. S. Birch. Sound absorption metasurface with symmetrical coiled spaces and micro slit of variable depth. *Applied Acoustics*, vol. 183, pp. 108312, 2021.